*Annals of Biomedical Engineering*, Vol. 23, pp. 346–358, 1995
Printed in the USA. 

0090-6964/95 $10.50 + .00


# New Models of the Oculomotor Mechanics Based on Data Obtained with Chronic Muscle Force Transducers

K. D. PFANN, E. L. KELLER, and J. M. MILLER

Smith-Kettlewell Eye Research Institute, San Francisco, CA, Graduate Group in Bioengineering, University of California, Berkeley, Berkeley, CA

**Abstract**—Several phenomenological models of the oculomotor mechanics that produce saccadic eye movements have been developed. These models have been based on measurements of macroscopic muscle and orbital tissue properties and measurements of eye kinematics during saccades. We recorded the forces generated by the medial and lateral recti during saccades in an alert, behaving monkey using chronically implanted force transducers. With this new data, we tested the ability of the classic saccade models to generate realistic muscle force profiles. Errors in the predictions of the classic saccade models led to a reexamination of the current models of extraocular muscle. Both a phenomenological, Hill-type muscle model and an approximation to Huxley's molecular level muscle model based on the cross-bridge mechanism of contraction (distribution moment model) were derived and studied for monkey extraocular muscle. Simulations of the distribution moment model led to insights suggesting (i) specific modifications in the lumped force/velocity relationship in the Hill-type model that resulted in this type of phenomenological model being able to generate realistic dynamics in extraocular muscle during saccades; (ii) the distribution of activity in the different fiber types in extraocular muscle may be central to the characteristics exhibited by the muscle during saccades; (iii) the transient properties of lengthening muscle such as yielding are not significant during saccades; and (iv) the series elastic component in active muscle may be predominantly generated by the elastic properties of the cross-bridges.

**Keywords**—Saccade, Extraocular muscles, Muscle cross-bridge models, Biomechanics.

## INTRODUCTION

The orbit and extraocular musculature involved in horizontal eye movements have been modeled by several investigators (for a review see Ref. 28). In general, most models have been phenomenological models with the same basic structure: two Hill-type muscle models attached to a second order linear model of the orbit. Throughout this paper a Hill-type muscle model refers to a lumped-parameter mechanical circuit model consisting of a series elastic element cascaded with a parallel combination of a force generator and a nonlinear viscous element (16). The research guiding the development of these phenomenological models was the measurement of steady-state, macroscopic muscle properties primarily in human strabismus patients (6,29), cats (2,5,26), and monkeys (12), and the measurements of eye kinematics (1,9). In the biomechanical studies cited, the parameters of the mechanical models were estimated from measurements that included the passive muscle length-tension relation, the active muscle length-tension relation, and the series elasticity relationship. In addition, the inertia of the globe was estimated, and the elasticity and damping constants of the human orbit were estimated with the medial and lateral recti detached.

The Hill-type model can generate realistic eye position, velocity, and acceleration trajectories for saccadic eye movements (20), which exhibit the most demanding ocular dynamics to model due to their extremely high velocities and accelerations. Even so, with the available measurements, models of this class are still under-determined (28). With the advancement of technology and the resulting availability of biocompatible materials, it is now possible to implant chronically force transducers on each of the horizontal recti and subsequently measure the individual muscle forces during normal saccadic eye movements in the alert, behaving monkey (22). In light of the new data provided by these force transducers, we have reexamined the existing models to see if they predict realistic muscle force records.

In this paper, we begin by comparing simulation profiles generated by a particular version of phenomenological model for horizontal saccadic eye movements (20) with eye position, velocity, and muscle force profiles recorded during horizontal saccades in the monkey. To this end, we (i) describe the methods used to record data from the monkey; (ii) describe the specific phenomenological model simulated (details given in Appendix A); and (iii) compare the simulated outputs to the data. Then we more closely examine the isolated muscle portion of the Hill-

This work was supported by National Institutes of Health Grants EY06860, EY06973, and EY06883.

Present address of K. D. Pfann: School of Kinesiology, University of Illinois at Chicago, 901 W. Roosevelt, Chicago, IL.

Address all correspondence to Dr. E. Keller, Smith-Kettlewell Eye Research Institute, 2232 Webster Street, San Francisco, CA 94115.

*(Received 5Aug94, Revised 15Dec94, Revised, Accepted 16Dec94)*

type model used in our initial simulations of the horizontal saccadic system. This leads us to (i) introduce a second muscle model, one based on the cross-bridge mechanism of contraction (34); (ii) describe this second model (details given in Appendix B); (iii) show results from simulations of the cross-bridge model that are then used to introduce appropriate changes in the phenomenological model to allow it to generate physiologically realistic behavior; and (iv) discuss insights about the properties of extraocular muscle derived from the models. We conclude with some final remarks.

## PHYSIOLOGICAL METHODS

One adult male *Macaca fascicularis* was utilized to obtain the data on muscle forces reported in this study. All experimental protocols were approved by the Institutional Animal Care and Use Committee at the California Pacific Medical Center and complied with the guidelines of the Public Health Service policy on Humane Care and Use of Laboratory Animals. The animal was prepared for eye movement recordings by implanting a scleral eye coil and head restraint system under sodium pentobarbital anesthesia and aseptic surgical conditions. Heart rate, respiratory rate, and body temperature were monitored for the duration of the surgery. Analgesics and antibiotics were given during the postsurgical recovery period. A coil of Teflon-coated stainless steel wire was implanted under the conjunctiva of the left eye using the procedure of Fuchs and Robinson (13), as modified by Judge *et al.* (19). A stainless steel tube was embedded in dental acrylic attached securely to the animal's skull with bone screws, permitting painless restraint of the animal's head during the experimental sessions. The scleral eye coil, when used in conjunction with a pair of orthogonally aligned magnetic fields maintained electronically in temporal quadrature, produced an eye position measurement system with a sensitivity of 0.25°, zero drift, and a bandwidth of 1 kHz (25). The monkey was returned to its home cage to recover from these surgical procedures and, following complete recovery, was trained to climb voluntarily from its cage into a primate chair for daily experimental sessions.

Prior to implantation of the force transducers, the monkey was trained to make saccades to lighted LEDs selected randomly from a grid array. An array of 25 LEDs was used consisting of five rows with LEDs spaced at 10° intervals ranging from ±20° from primary position along both the vertical and horizontal meridians.

When the animal had learned to make accurate saccades to the location of the lit LED, a buckle force transducer was implanted on the left lateral rectus (LR), and about 4 months later one was implanted on the left medial rectus (MR). To implant the transducer, the muscle was exposed but not detached (22). The transducer was sutured to the muscle to prevent rotation. The signal leads led out of the orbit under the skin and exited through a connector attached to the acrylic cap. The globe was rotated to ensure the leads were not limiting motion.

After the monkey recovered, muscle forces and eye position were measured during saccades and were sampled at 1000 Hz and stored on computer disk. The trials were sorted, and successful trials of horizontal saccades were examined. Eye position records were smoothed and digitally differentiated. Force records were scaled as a percentage of the total range observed in each muscle during the session; the range and distribution of movements were similar across sessions. Complete details on the physiological database, which includes hundreds of saccades made to all positions in the LED array including many examples of individual eye movements and simultaneous muscle force measurements, have been published already (22,23). For the purpose of this modeling paper, we concentrate on the data from four consecutive sessions in order to minimize the effects of possible slow changes in force transducer sensitivity. This data included 60 horizontal saccades of amplitudes ~10° and 20° in both directions.

When one of the transducers failed, the monkey was euthanized with an overdose of pentobarbital.

## DESCRIPTION OF THE PHENOMENOLOGICAL MODEL

The phenomenological model of the monkey horizontal saccadic mechanics used in this study was derived from the human model developed by Lehman and Stark (20), which has been shown to produce realistic eye position, velocity, and acceleration trajectories of human saccades initiated from primary position over a range of saccade sizes. Moreover, the Lehman and Stark model incorporates the results of several generations of model development and has been extensively analyzed and subjected to rigorous sensitivity analyses (3,9,17). To directly compare the force profiles predicted by this model to those recorded in the monkey, it was necessary to first convert the model based on human data to reflect the mechanics of the monkey musculature and orbit. In addition, to compare the forces recorded with those predicted by the model, it was essential to first divide the total passive elasticity into its components, which consist of the passive muscle elasticities and the orbital elasticity in parallel. A mechanical circuit of the modified model used in this study is shown in Fig. 1. The muscles are modeled with a variation of the Hill muscle model, the parameters for which are derived mostly from steady-state measurements of macroscopic muscle properties. Briefly, the reciprocally organized neural inputs ($I_1$ and $I_2$) are filtered to generate the "active state" internal muscle forces, $F_{a1}$ and

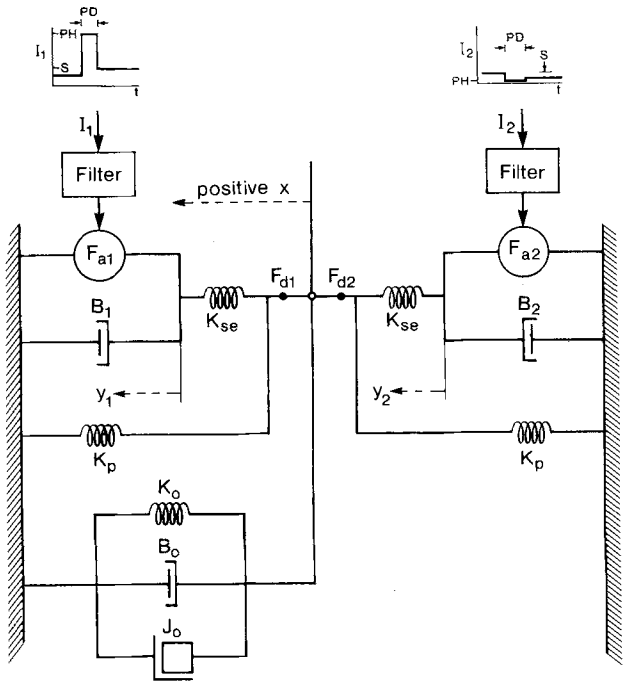


**FIGURE 1. Mechanical circuit model of the horizontal saccadic eye movement system. The phenomenological model simulated in this study is shown. The orbital mechanics are modeled by a linear mass-spring-dashpot system ($K_o$, $B_o$, $J_o$). The muscles are modelled as follows: The inputs ($I_1$, $I_2$) are the neural inputs converted to their force equivalents. The "active state force" of each muscle ($F_{a1}$, $F_{a2}$) is a filtered version of its input and is represented by a force generator. Each force generator is in parallel with an non-linear viscous element ($B_1$, $B_2$) representing the force-velocity relationship of the muscle. This combination is in parallel with a series elastic element ($K_{se}$). The whole combination is in parallel with another spring representing the passive muscle elasticity ($K_p$). The insets at the top show the temporal waveforms for the inputs: PD indicates pulse or pause duration, PH indicates pulse or pause height and S indicates the level of the final steady-state step.**

$F_{a2}$. In each muscle, the force generator is in parallel with a nonlinear dashpot, $B$, which represents the force-velocity relation of active muscle. This unit is in series with an elastic element, $K_{se}$, which represents the experimentally measured property that an instantaneous reduction in load results in an instantaneous change in muscle length (*i.e.*, the characteristic of a spring). This group of mechanical elements is in parallel with an elastic element, $K_p$, which represents the passive elastic properties of the muscle. Two of these muscle models are combined with a mass-spring-dashpot representation of the orbit to model the horizontal saccadic system.

This type of lumped parameter model of the macroscopic properties of muscle is appealing because the parameters can be measured relatively easily and because the structure gives insight into the behavior of the muscle during movement. On the other hand, the model allows no comparisons to be made with the underlying mechanism of contraction. Moreover, it does not represent all the known transient properties of lengthening muscle, which may be important especially in high-velocity movements like saccades. (The force-velocity relationship used in the model is a function of velocity for a given level of innervation, whereas lengthening muscle has been shown to exhibit yielding (34), which implies that force in the relationship cannot be uniquely described by velocity and innervation.)

The model was simulated with Simnon, a nonlinear dynamic systems simulation package. The parameters and the equations of motion for this model of the monkey horizontal saccadic system are derived in Appendix A.

## RESULTS

Figure 2 shows experimentally measured eye position and velocity profiles (upper two sections), agonist force and force rate profiles (middle two sections), and antagonist force and force rate profiles (lower two sections) recorded during a 10° (dashed) and a 20° (solid) temporally directed saccade. Each trace shown in this figure is obtained from one representative saccade of each size selected from the sample of 60 similar movements. We believed that it was more realistic to optimize the model parameters to attempt to create actual individual movements rather than averaged results. However, having optimized the model for the particular movements shown in Fig. 2, we then checked to see if the model could also produce each of the 60 movements included in the data-

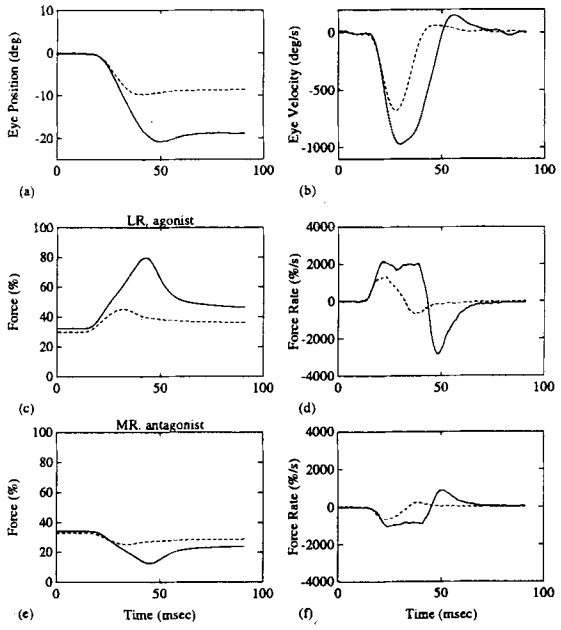


**FIGURE 2. Trajectories recorded from a monkey during horizontal saccadic eye movements. Eye position (a) and velocity (b), agonist force (c) and force rate (d), and antagonist force (e) and force rate (f) recorded during a 10° (dash) and 20° (solid) temporally directed saccade initiated from primary position.**

base. In order to provide assurance that the selected movements are indeed representative of the data we measured the standard errors of the mean position reached at the end of the 10° and 20° saccades and the standard errors for the muscle force measurements at the points of maximum rate of force change during 10° and 20° saccades. The standard error values obtained from the calculations were ±0.71° and 0.88° for position and ±0.94 and 3.75% for force for 10° and 20° movements, respectively.

The normalized magnitudes of the forces exerted by the muscles are shown on this figure because they are adequate for the comparisons being made here. The estimation of the absolute values of muscle forces is discussed in Appendix C. Figure 3 shows analogous waveforms but now generated by simulations of the model for monkey saccadic eye movements, and Fig. 4 shows a direct comparison of the overlaid normalized experimental data and normalized model force profiles. The eye kinematic traces show that, as was the case for the human (20), the model for the monkey can be optimized to produce very realistic eye position and velocity profiles. The most obvious feature found in the experimental muscle force records is the qualitative symmetry in the shape of the agonist and antagonist force trajectories. In contrast, the simulated force profiles from the model show a definite asymmetry between agonist and antagonist muscle trajectories. By varying the parameters of the inputs ($I_1$, $I_2$) to the model the shape of the agonist profile, for example, can be made to look more like that recorded from the monkey; however,

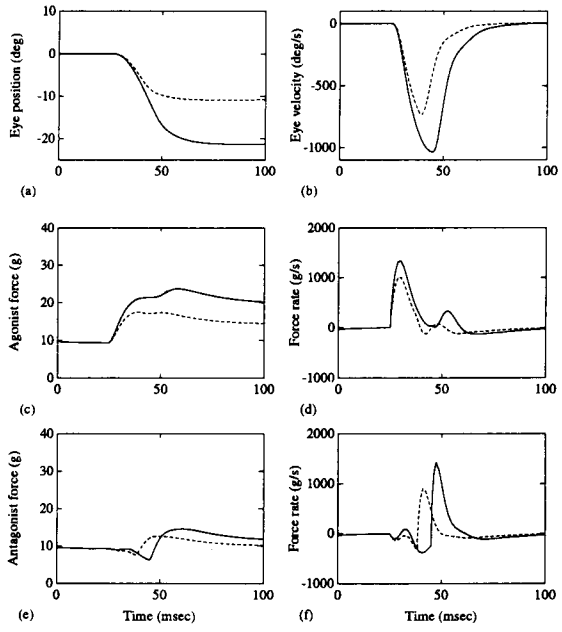


**FIGURE 3. Trajectories generated by the model of monkey saccadic eye movements. Eye position (a) and velocity (b), agonist force (c) and force rate (d), and antagonist force (e) and force rate (f) recorded during a 10° (dash) and 20° (solid) saccade initiated from primary position.**

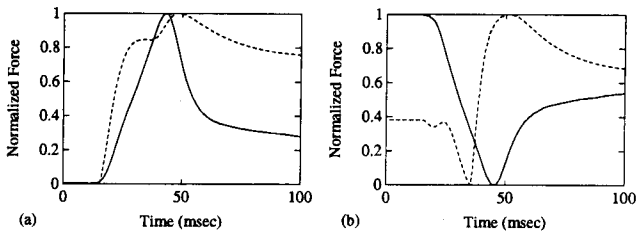


**FIGURE 4. Comparison of normalized force profiles from data and model. Normalized agonist (a) and antagonist (b) force profiles from data (solid) and model simulations (dash) for a 20° temporal saccade initiated from primary position.**

the resulting antagonist profile looks even more unrepresentative of the monkey data. No simple parameter modifications change this result. In spite of generating reasonable position and velocity profiles, in its present form the model does not accurately reflect the force dynamics of the extraocular muscles during horizontal saccadic eye movements. This could be due to errors in the model of the muscles, of the orbit, and/or of innervation. The muscle model is a good choice to study more closely with an eye for possible changes because (i) the force-velocity relation is poorly characterized, at least for lengthening muscle, (ii) the series elasticity is assumed to be constant in spite of evidence suggesting otherwise (28), (iii) the required input forces ($F_a$) are higher than physiologically measured forces (12), and (iv) the orbital model is thought to be accurate in the range of movements being studied here (28).

## DESCRIPTION OF A MECHANISTIC MODEL OF EXTRAOCULAR MUSCLE

For a muscle model to be useful in studies of movement on a macroscopic scale, the model (i) should not require too much computation time and (ii) must accurately represent the characteristics of whole muscle during movements that include both lengthening and shortening under variable levels of innervation. Hill-type models are commonly used because they easily satisfy the first requirement and, to some extent, satisfy the second. However, the model does not exhibit known transient properties of lengthening muscle such as yielding. For this reason, it may not be a useful representation for high-velocity movements like saccades, which presumably, produce transient behavior to the greatest extent. This provides the clearest motivation for more closely examining the ability of the muscle model to exhibit the dynamics of extraocular muscle during saccadic eye movements.

Another muscle model, the distribution moment (DM) model (34), was studied along with the Hill-type model for comparison purposes because it does exhibit some of the transient properties of lengthening muscle, while remaining computationally feasible. The DM model is based

on the molecular mechanism of contraction rather than a lumped functional representation of macroscopic muscle properties. The macroscopic muscle characteristics for this type of model are an emergent property.

A. F. Huxley proposed a muscle model based on the mechanism of contraction, or cross-bridge formation and detachment (18). In this case, the muscle is assumed to consist of a large number of identical sarcomeres, so the macroscopic muscle characteristics can be directly determined from the model of a single sarcomere.

Figure 5 shows a schematic of the two-state Huxley model for one sarcomere. Each of the large number of cross-bridges in a muscle is represented by a spring, and the force generated by each cross-bridge is proportional to the length of its spring ($x$). A change in muscle length is generated by the movement of the myosin heads in a cross-bridge (bond), which forces the myosin and actin fibers to slide past each other in opposite directions. If, at a given moment, the distribution of bond lengths, or spring lengths—$n(x, t)$—is known, then the total force generated by the muscle can be calculated. In a simple two-state kinetic model with a constant level of innervation, we only need to know the rates of bond attachment ($f$) and detachment ($g$) to write a partial differential equation describing the rate of change of the bond distribution in one-half sarcomere:

$$\frac{\partial n(x, t)}{\partial t} - v(t)\frac{\partial n(x, t)}{\partial x} = f(x)\,[1 - n(x, t)] - g(x)n(x, t)$$

where $n(x, t)$ is the bond distribution, $0 < n < 1$; $v(t)$ is the velocity of shortening; $f(x)$ is the rate of bond attachment; and $g(x)$ is the rate of bond detachment.

Zahalak suggested an approximation that makes the simulation of this equation computationally tractable (34). First, he noted that the partial differential equation can be rewritten as an infinite series of ordinary differential equations of the moments of the distribution. Further, he showed that if the shape of the function describing the bond distribution is known *a priori* and if the function is completely described by a finite number of its moments, the system can be expressed as a finite series of coupled, first order differential equations. He assumed the bond distribution was Gaussian, in which case the dynamics can be expressed with three differential equations (because the first three moments completely define a Gaussian distribution). Conveniently, the macroscopic muscle properties of interest are functions of these low order moments. The parameter values and defining equations for the DM model of a monkey extraocular muscle are given in Appendix B.

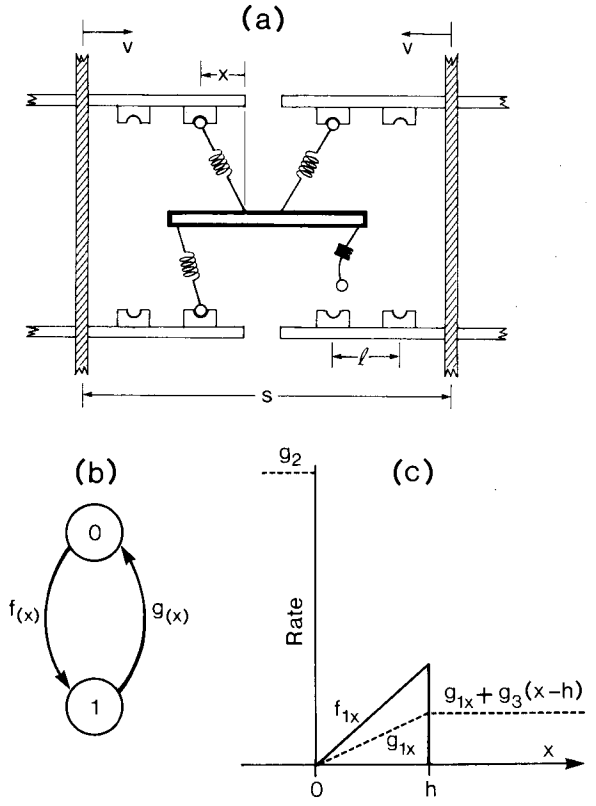


**FIGURE 5. Schematic of the cross-bridge model of muscle contraction. (a) shows a schematic of cross-bridges in a sarcomere. A myosin filament is represented by the thick bar and actin filaments are represented by the thin bars. The vertical bars represent Z lines. Cross-bridge sites are represented by balls attached to the myosin filament by springs. Actin sites are represented by the matching sockets. The figure shows both attached and unattached cross-bridges. *x* reflects the length of an attached spring; *v* is the velocity; *l* is the distance between actin sites; and *s* is the sarcomere length. (b) shows the two-state model of cross-bridge formation in which State 0 is the unattached and State 1 the attached condition. *f* is the attachment rate constant and *g* is the detachment rate constant. (c) shows the rates of attachment and detachment as a function of *x*. See text for the definition of symbols in (c).**

*Methods for Comparing the Muscle Models*

The approach taken to compare the two classes of models was to calculate the input necessary to generate the recorded force trajectories, given the muscle length and velocity derived from the simultaneously recorded eye position data. It is important to recognize that the inputs to the two muscle models cannot be directly compared because the input to the Hill model is active state and the input to the DM model is activation of cross-bridge sites. However, their temporal shapes and the similarity of these shapes can be compared with those reported for motoneuronal firing patterns in monkey (11,14,27,30) that ultimately generate both model inputs.

Before the data could be used with the simulations, absolute magnitudes of force had to be estimated from the recorded data. Because the muscle force amplifiers were modified early in the course of the experiments (but well before any of the data used in the present report were

obtained), we could not directly compare the original calibrations to the recorded data to determine absolute forces. Instead, we estimated forces as described in Appendix C.

Both the Hill-type and DM muscle models were simulated. For simplicity, the passive elasticity was assumed to be zero in both models even though it makes a small contribution at the extremes of the range of eye movements explored (±20°) (6). The inverse models were simulated using Borland C/C++. Recorded force and position records were used as input and the optimal muscle activation profiles were calculated using a modified version of "brent.c" optimization algorithm (24). The optimization was checked by running forward simulations with the calculated activation and the recorded position as input and verifying that the model forces matched the recorded forces. Note that any parameters derived with the direct aid of simulation were derived for one particular saccade trial (*e.g.*, those shown on Fig. 3) and then were used in simulations with data from other 60 saccade trials. Also, the optimal active state in the Hill model (*i.e.*, $F_{a1}$ and $F_{a2}$ in Fig. 1) was calculated instead of the unfiltered inputs ($I_1$ and $I_2$ in Fig. 1).

As described in Appendix B, $g_l$, which partially defines the rate of cross-bridge detachment, was first calculated to satisfy the relationship Hill found between maintenance heat, maximum isometric force, and maximum velocity of shortening. Simulations suggested this was an appropriate $g_l$ for the agonist muscle. However, the simulations also suggested that different values of this parameter were needed for agonist and antagonist muscle. A relatively large $g_l$ is needed to allow the agonist force rate to decrease rapidly after peak force is reached early in the saccade. If $g_l$ is too low, muscle activation has to decrease more rapidly and to a larger extent to compensate for the slow rate of detachment; as a result, agonist muscle activation dips well below the final steady-state activation level (pulse-negative pulse-step), which contradicts the known pulse-slide-step firing patterns of ocular motoneurons (11,14,27,30). In contrast, in the antagonist muscle, if $g_l$ is too high, then muscle activation must decrease slowly throughout most of the saccade instead of "turning off" in the pause-slide-step pattern of ocular motoneurons. The use of different detachment rates for agonist and antagonist muscles is consistent with our basic understanding of extraocular muscle. The large fast fibers are thought to dominate force generation in the agonist muscle (even though all fibers contribute). In contrast, at the lower levels of innervation in the antagonist muscle, the slow fibers are believed to contribute a much larger proportion of the force (31); moreover, slow fibers have a slower rate of decay in force, which, presumably, corresponds to a lower rate of cross-bridge detachment and would, therefore, be the limiting factor in the rate at which the antagonist muscle force decreases during a saccade.

The detachment rate factor $g_l$ has an effect on the force-lengthening velocity that can also be represented in the Hill muscle model by scaling the lengthening force-velocity relationship differently for the agonist and antagonist muscle (*i.e.*, different $d_{len}$, which is defined in Appendix A). Simulations showed that analogous modifications of $d_{len}$ had the same effect on the calculations of agonist and antagonist activations in the Hill model as does varying $g_l$ in the DM model. Because the larger saccades of the monkey used in the present study tended to overshoot the target and then return with a small dynamic movement, the agonist muscle has a brief period of lengthening at the end of the saccade. As a result, the lengthening force-velocity relationship clearly affects the agonist muscle characteristics as well as the antagonist. However, the results also applied to smaller saccades with little overshoot. In the agonist muscle, $d_{len}$ must be large or else a pulse-negative pulse-step activation pattern is required; a large "braking pulse" in agonist activation at the end of a saccade is not consistent with the observed pulse-slide-step pattern of single motoneurons (14). In contrast, in the antagonist muscle, $d_{len}$ must be small or else a slowly decreasing activation is predicted, which is inconsistent with the pause-slide-step pattern of motoneurons. The larger $d_{len}$, the smaller the force at a given lengthening velocity and level of innervation. Decreasing $d_{len}$ has a similar affect on the lengthening force-velocity relationship as increasing $g_l$ in the DM model.

## RESULTS FROM MUSCLE MODEL SIMULATIONS

Figures 6 and 7 show the DM and modified Hill model predictions of agonist and antagonist muscle activation for 10° and 20° saccades from primary position (d,f) as well as the forces (c,e) and eye kinematics (a,b) produced during those saccades. Recall that the force and kinematic trajectories were the inputs used to calculate the appropriate muscle activations.) The modified Hill model utilized different values of the parameter $d_{len}$ as described above and in Appendix A for the agonist and antagonist muscles. With this modification in place the predicted muscle activations are similar for the two models and both are consistent with known motoneuronal activations during saccades; their durations are nearly the same as saccade duration (11,14,27,30). Agonist activation is much greater for 20° saccades than 10° saccades. At the same time, motoneuron burst frequency is higher and longer in duration during 20° saccades than during 10° saccades. As a result, one would expect muscle activation to increase for a longer time and to a greater extent during the larger saccades. Antagonist activation is consistent with motoneurons being "turned off" (pause) or reduced to a very low firing rate. Antagonist activation decreases at about the same rate; activation for 10° saccades appears to begin

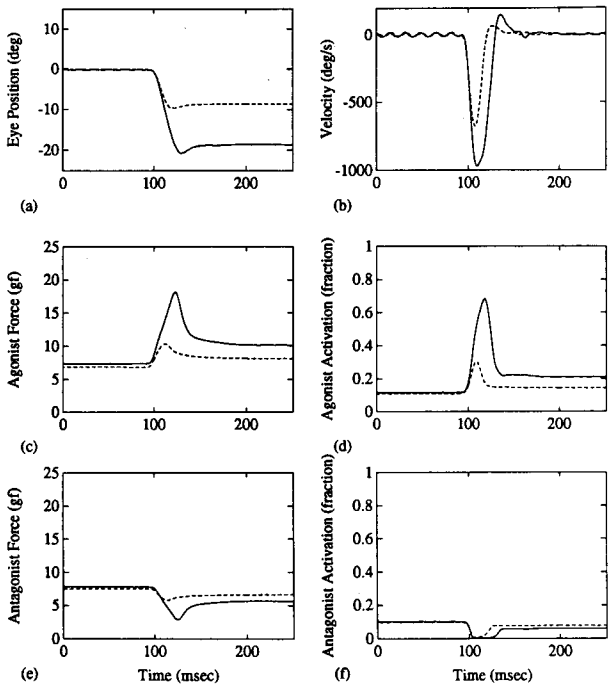


**FIGURE 6. Computed activations of DM model for 10° and 20° saccades initiated from primary position. Eye position (a) and velocity (b), agonist and antagonist forces (c,e) and agonist and antagonist activations (d,f) during 10° (dash) and 20° (solid) saccades initiated from primary position are shown. The activations were calculated so the DM model generated the measured force profiles given the measured kinematics.**

to return to its tonic level just before the minimum activation is reached, whereas activation for 20° saccades plateaus at the minimum.

## DISCUSSION

### *Force-Velocity Relationship*

It was somewhat surprising that the modified Hill-type model produced activation patterns so similar to the DM model. The modification in the Hill model that produced this result (*i.e.*, requiring $d_{len}$ to have different values for the agonist and the antagonist) appeared at first to be merely a mathematical manipulation without any connection to actual properties of the muscle. However, simulations of the DM model suggested a connection between the manipulation and the fact that agonist and antagonist eye muscles are likely to be dominated by physiologically different muscle fiber types, the fast and slow types, respectively. Since no details about the contractile properties of these two types eye muscle fibers exist, our simulation results suggest the need for explorations of the force-velocity properties of different fiber types within extraocular muscle as well as the force-velocity relationship of extraocular muscle for varying degrees of innervation. The results presented here suggest, at the very least, that the force-lengthening velocity relationship is important in the simulation results.

The DM and Hill models that we have developed have similar force-velocity relationships for shortening muscle but not for lengthening muscle. Even the steady-state force-lengthening velocity relationships are not the same for these two models. However, the exact shape of the assumed force-lengthening velocity relationship did not appear to significantly affect the simulations in the Hill model (several hyperbolas and straight lines with various slopes were used but produced little change in the simulated results).

We used simulations of the DM model to investigate the transient properties of rapidly lengthening extraocular muscle. The simulations showed that the yielding that resulted from sudden changes in lengthening velocity lasts only about 5–7 msec and is small in magnitude. The high rate of attachment accounts for the rapid recovery. The importance of transient properties does not appear to be as great as anticipated, at least with the rate parameters assumed ($f[x]$ and $g[x]$). The simulations agree with the experimental results: the muscle forces do not show unusual transient properties; instead the antagonist muscle always shows a smooth change, qualitatively symmetrical to the agonist force trajectory. It appears that the transition

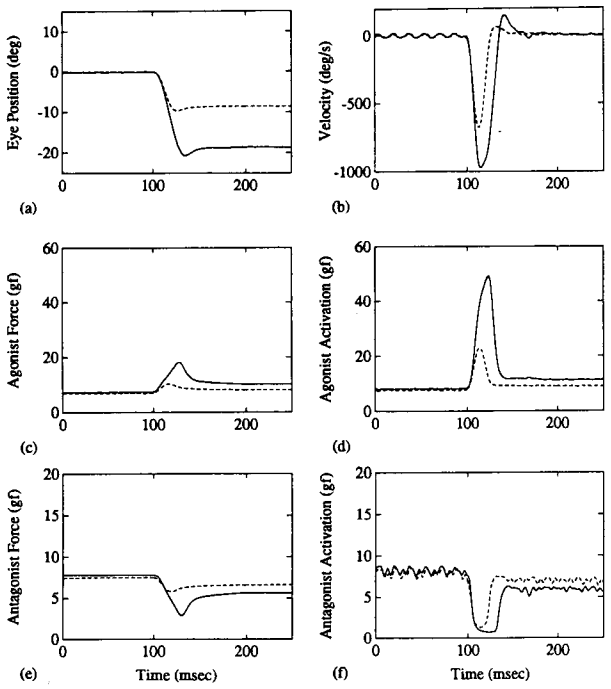


**FIGURE 7. Computed activations of modified Hill model for 10° and 20° saccades initiated from primary position. Eye position (a) and velocity (b), agonist and antagonist forces (c,e) and agonist and antagonist activations (d,f) during 10° (dash) and 20° (solid) saccades initiated from primary position are shown. The activations were calculated so the modified Hill model generated the measured force profiles given the measured kinematics.**

to high speeds during saccades is smooth enough that yielding does not occur. The DM model exhibits yielding when the steady-state velocity is suddenly changed but not when saccadic velocity profiles are assumed.

*Series Elasticity*

The series elastic element is included in the Hill model to represent the result of quick release experiments. When the force applied to an activated, isometric muscle is suddenly reduced, the muscle length exhibits an abrupt reduction in length followed by a more gradual reduction until a new steady-state length is reached. The series elasticity is often attributed to the tendon, which is made of elastic, collagenous tissue. However, a quick estimate of the stiffness of tendon suggests that this is an unlikely explanation: Young's Modulus for collagen (32),

$$E_{ten} = 10^{10} \text{ dyne/cm}^2 = 10^7 \text{ gf/cm}^2$$

tendon stiffness,

$$K_{ten} = E_{ten}A_{ten}/L_{ten}$$

where $A_{ten}$ is the cross-sectional area of tendon; $L_{ten}$ is the length of tendon. (We assumed $L_{ten} = 0.6$ cm (19) and $A_{ten} = A_{mus}/4 = 0.024$ cm$^2$, we assumed the tendon has a relatively large cross-sectional area since it has a wide insertion.)

$$K_{ten} = 3.92\text{e}8 \text{ dyne/cm} = 6{,}480 \text{ gf/deg}$$

In contrast, series elasticity, $K_{se} = 2.3$ gf/deg (see Appendix A) = 1.4e5 dyne/cm, which implies that $K_{ten} \gg K_{se}$. Since tendon stiffness is three orders of magnitude greater than the series spring stiffness for these muscles, the elasticity must be in the muscle itself.

The most likely location for the series elasticity is in the cross-bridges, although elastic, connective tissue throughout the muscle may also contribute. Cross-bridge sites are the only mechanical elements in muscle that can directly account for experimental results that show the magnitude of the series elasticity varies with innervation (5). Fortunately, the DM model can be used to explore this possibility since muscle stiffness is proportional to the zeroth moment of the bond distribution and is derived as follows:

$$K_{1/2\text{-}sarc}(t) = \frac{msk}{21}\int_{-\infty}^{\infty} n(x, t)dx = \frac{mskh}{21}Q_0(t)$$

where $K_{1/2\text{-sarc}}$ is the half-sarcomere time varying stiffness and the parameters are defined in Appendix B. The total muscle stiffness is the half-sarcomere stiffness times the number of half-sarcomeres in parallel divided by the number of half-sarcomeres in series, or:

$$K_{mus}(t) = \frac{A_{pp}ms_{pp}kh}{4ln_s}Q_0(t) = \frac{A_0}{2n_s}\kappa_{1/2\text{-}sarc}$$

where $K_{mus}(t)$ is the instantaneous muscle stiffness.

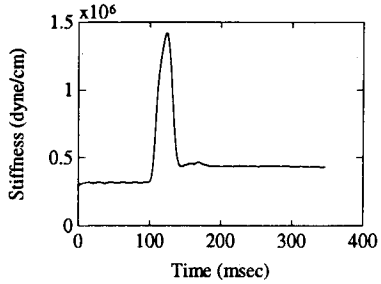


**FIGURE 8. DM model simulation of muscle series elasticity during a 20° saccade from primary position.**

Figure 8 shows the instantaneous muscle stiffness during a 20° saccade from primary position. Note that the stiffness is the same order of magnitude as that expected from experimental measurements. Therefore, the DM simulations support the idea that the series elasticity of extraocular muscle is primarily in the cross-bridges.

*Final Conclusions and Remarks*

One can generate many different models with the same input/output characteristics. Therefore, the purpose of the model must be considered. For example, in this study extraocular muscle is modeled to further our understanding of the oculomotor system. Therefore, the structure of the system is important. Another model with the same input/output characteristics would not be useful. The DM model is directly based on the mechanism of contraction and is, therefore, useful for making new associations between the data and the physiology. For example, it is certainly a more useful model if one is studying how a disease affects the system. However, the DM model is more complicated and computationally slower than the Hill model. The Hill model represents the macroscopic manifestations of the molecular interactions. With appropriate modifications in the Hill model, it also appears to reflect adequately the functional macroscopic components of extraocular muscle. As a result, our modified Hill model may be useful for additional simulation studies on a gross scale. For example, it could be used to explore the interactions of the six extraocular muscles and also nonlinear, initial position effects when eye movements are made from eccentric starting points.

## REFERENCES

1. Bahill, A. T., M. R. Clark, and L. Stark. The main sequence, a tool for studying human eye movements. *Math. Biosc.* 24:191–204, 1975.
2. Barmack, N. H., C. C. Bell, and B. G. Rence. Tension and rate of tension development during isometric responses of extraocular muscles. *J. Neurophysiol.* 34:1072–1079, 1971.
3. Clark, M. E., and L. Stark. Control of human eye move-

ments: I. modelling of extraocular muscle. *Math. Biosc.* 20:191–211, 1974.
4. Close, R. I., and A. R. Luff. Dynamic properties of inferior rectus muscle of the rat. *J. Physiol. Lond.* 236:259–270, 1974.
5. Collins, C. C. Orbital mechanics. In: *The Control of Eye Movements,* edited by P. Bach-y-Rita, C. C. Collins, and J. E. Hyde. New York: Academic Press, 1971, pp. 283–325.
6. Collins, C. C. The human oculomotor control system. In: *Basic Mechanisms of Ocular Motility and Their Clinical Implication,* edited by E. Lennerstrand and P. Bach-y-Rita, Oxford: Pergammon, 1975, pp. 145–180.
7. Collins, C. C., M. R. Carlson, A. B. Scott, and A. Jampolsky. Extraocular muscle forces in normal human subjects. *Invest. Ophthalmol. Vis. Sci.* 20:652–664, 1981.
8. Collins, C. C., D. O'Meara, and A. B. Scott. Muscle tension during unrestrained human eye movements. *J. Physiol. Lond.* 245:351–369, 1975.
9. Cook, G., and L. Stark. Dynamics of the saccadic eye-movement system. *Commun. Behav. Biol.* 1:197–204, 1968.
10. Fuchs, A. F. Saccadic and smooth pursuit eye movements in the monkey. *J. Physiol. Lond.* 191;609–631, 1967.
11. Fuchs, A. F., and E. S. Luschei. Firing patterns of abducens neurons of alert monkeys in relationship to horizontal eye movement. *J. Neurophysiol.* 33:382–392, 1970.
12. Fuchs, A. F., and E. S. Luschei. Development of isometric tension in simian extraocular muscle. *J. Physiol.* 219:155–166, 1971.
13. Fuchs, A. F., and D. A. Robinson. A method for measuring horizontal and vertical eye movement chronically in the monkey. *J. Appl. Physiol.* 21:1068–1070, 1966.
14. Goldstein, H. P. The Neural Encoding of Saccades of Rhesus Monkey. Baltimore: Johns Hopkins University, Ph.D. Thesis, 1983.
15. Goldstein, H. P., A. B. Scott, and L. B. Nelson. Ocular motility. In: Biomedical Foundations of Ophthalmology, vol. 2, edited by E. Tasman and U. Jaeger. New York: J. Lippincott, 1989, pp. 1–65.
16. Hill, A. V. The heat of shortening and the dynamic constants of muscle. *Proc. Roy. Soc.* 126B:136–195, 1938.
17. Hsu, F. K., A. T. Bahill, and L. Stark. Parametric sensitivity analysis of a homeomorphic model for saccadic and vergence eye movements. *Computer Prog. Biomed.* 6:108–116, 1976.
18. Huxley, A. F. Muscle structure and theories of contraction. *Prog. Biophys. Biophys. Chem.* 7:257–318, 1957.
19. Judge, S. J., B. J. Richmond, and F. C. Chu. Implantation of magnetic search coils for measurement of eye position: an improved method. *Vision Res.* 20:535–538, 1980.
20. Lehman, S., and L. Stark. Simulation of linear and nonlinear eye movement models: sensitivity analyses and enumeration studies of time optimal control. *J. Cybern. Info. Sci.* 4:21–43, 1979.
21. Miller, J. M., and D. Robins. Extraocular muscle sideslip and orbital geometry in monkeys. *Vision Res.* 27:381–392, 1987.
22. Miller, J. M., and D. Robins. Extraocular muscle forces in alert monkey. *Vision Res.* 32:1099–1113, 1992.
23. Pfann, K. D. Quantitative Studies of Eye Movement Generation: Biomechanics and Neural Control. San Francisco/Berkeley: University of California, Ph.D. Thesis, 1993.
24. Press, W. H., S. A. Teukolsky, W. T. Vetterling, and B. P. Flannery. *Numerical Recipes in C.* New York: Cambridge University Press, 1988, pp. 402–405.
25. Robinson, D. A. A method of measuring eye movement using a scleral search coil in a magnetic field. *IEEE Trans. Bio-Med. Eng.* BME-10:137–145, 1963.
26. Robinson, D. A. The mechanisms of human saccadic eye movement. *J. Physiol. Lond.* 174:245–264, 1964.
27. Robinson, D. A. Oculomotor unit behavior in the monkey. *J. Neurophysiol.* 33:393–404, 1970.
28. Robinson, D. A. Models of the mechanics of eye movements. In: *Models of Oculomotor Behavior and Control,* edited by B. L. Zuber. Boca Raton: CRC Press, 1981, pp. 21–41.
29. Robinson, D. A., D. M. O'Meara, A. B. Scott, and C. C. Collins. Mechanical components of human eye movements. *J. Appl. Physiol. 26:548–553, 1969.*
30. Schiller, P. H. The discharge characteristics of single units in the oculomotor and abducens nuclei of the unanesthetized monkey. *Exp. Brain Res.* 10:347–362, 1970.
31. Spencer, R. F., and J. D. Porter. Structural organization of the extraocular muscles. In: *Neuroanatomy of the Oculomotor System,* edited by J. A. Büttner-Ennever. Amsterdam: Elsevier, 1988, pp. 33–80.
32. Wainwright, N. W., C. D. Biggs, R. N. Currey, and R. S. Gosline. *Mechanical Design in Organisms.* Princeton: Princeton University Press, 1976.
33. Woledge, R. C., N. A. Curtin, and E. Homsher. *Energetic Aspects of Muscle Contraction.* New York: Academic Press, 1985.
34. Zahalak, G. I. A distribution-moment approximation for kinetic theories of muscular contraction. *Math. Biosci.* 55:89–114, 1980.

## APPENDIX A

This appendix describes the parameter derivations for the Hill-type model of the monkey horizontal saccadic system and the equations used to simulate the model. The following symbols will be used: $K$ is an elasticity, $B$ is a viscosity, $J$ is a moment of inertia, $A$ is cross-sectional area, $R$ is the globe radius, $L$ is muscle length, $V_{max}$ is the maximum velocity of shortening of the muscle, superscript $^M$ denotes a monkey model parameter, superscript $^H$ denotes a human model parameter, subscript $_o$ denotes an orbit parameter. If no superscript is used, the parameter is for the model of monkey saccades. Figure 1 shows the topological arrangement of the lumped mechanical elements in the model.

The values of the parameters for the monkey orbital mechanics in the present paper are mostly derived directly from monkey data or estimated by scaling human data (7,8,29). In the monkey the extraocular muscles are shorter, 20 mm (21) compared with 40 mm (15) and smaller in cross-sectional area, 9 $mm^2$ (21) compared with 16.9 $mm^2$ (15). Also, the globe is smaller, 9.3 mm radius (21) compared with 11 mm (5). Finally, monkey saccades are faster than the same size human saccades (1,10). The moment of inertia of the monkey orbit was derived by approximating the globe as a rigid sphere of radius 9.3

mm (20) and density 1 g/ml: $J_0^M = 2.88e-5$ gf sec$^2$/degree. In the Lehman and Stark human model (20), the parameters representing the passive viscoelasticity of the orbit are the lumped effects of the optic nerve, orbital fat, the other extraocular muscles, other surrounding tissue, and the passive elasticity of the medial and lateral recti. However, to compare the forces recorded with those predicted by the model, we must separate the contribution of the medial and lateral recti to the passive elasticity. The orbital elasticity has been measured in humans with the medial and lateral recti detached and was found to be $K_o^H = 0.5$ gf/degree (29). We assumed that the tissue contributing to the elasticity was proportional to the surface area of the globe, so passive elasticity was scaled by the ratio of the surface areas of the globes and viscosity was scaled such that the viscoelastic time constant ($B/K$) remained the same as that estimated for humans (20): $B_o^M = 0.01$ gf sec/degree, $K_o^M = 0.35$ gf/degree.

The passive elasticity of the medial and lateral recti were separated so that the model could predict total muscle force for comparison with the measured data. The force contribution of the passive muscle elasticity was estimated by fitting the following equation to data of the passive length-tension curve of the monkey medial rectus (12):

$$F_p^M = a^M \cdot (x + 25)^2, \quad x > -25°$$
$$0, \quad \text{otherwise}$$

where, $F_p^M$ (gf) is the passive muscle force, $a^M = 0.001975$ gf/degree$^2$ is a constant, and $x$ (degrees) is eye position (positive is temporal). A symmetric equation was used for the lateral rectus. Note that even though the individual passive muscle elasticities are nonlinear, the nonlinearities tend to cancel each other such that the parallel combination is quasilinear (29).

Human muscle series elasticity was estimated from quick release experiments on human extraocular muscle (8). Since elasticity should increase with area (analogous to parallel springs) and decrease with length (analogous to series springs), the series elasticity was scaled from the human to the monkey; at the same time, it was scaled relative to the size of the globe (since the units used in the model are per degree not per millimeter):

$$K_{se}^M = K_{se}^H \cdot \frac{A^M}{L^M} \cdot \frac{L^H}{A^H} \cdot \frac{R^H}{R^M}$$

where $K_{se}^M = 2.3$ gf/degree, $K^H{}_{se} = 1.8$ gf/degree, $A^M = 9$ mm$^2$, $A^H = 16.9$ mm$^2$, $R^M = 9.3$ mm, $R^H = 11$ mm, $L^M = 20$ mm, $L^H = 40$ mm.

The nonlinear viscosities in the model ($B_1$, $B_2$) characterize the force-velocity relationship of muscle, which was derived from experimental work on skeletal muscle in other animals. It had been shown that tetanized muscle shows a hyperbolic force-velocity relationship during shortening, and the parameters describing the asymptotes of the hyperbola are related to the muscle's maximum rate of shortening ($V_{max}$) and maximum isometric force ($F_0$) (16). The maximum rate of shortening for the monkey model was estimated by scaling the data for human extraocular muscle by muscle length and globe radius (the latter is necessary because the maximum velocity is in units of degrees/sec:

$$V_{max}^M = V_{max}^H \cdot \frac{L^M \cdot R^H}{L^H \cdot R^M}$$

where $V_{max}^M = 2200$ degrees/sec, $V_{max}^H = 3600$ degrees/sec. Moreover, the whole force-velocity relationship was assumed to scale with activation.

Finally, the neural inputs ($I_1$, $I_2$) were similar to those used in the human model (20) (*i.e.*, the pulse-step pattern [27]). The pulse and pause durations (PD in Fig. 1) were assumed to be half the duration of the saccade; the pulse or pause height (PH) is scaled nonlinearly with saccade magnitude; and the step level (S) is scaled with saccade magnitude. Finally, the innervation envelopes are filtered with first-order lags and converted into an equivalent active state force. Because monkey saccades are faster, the inputs and filtering had to be modified: pulse and pause duration (PD) = 0.5 · saccade duration = 12.5 msec (10°), 20 msec (20°); fixation forces and equivalent input were scaled by cross-sectional area (0.5) so agonist step (S) = (8 + 0.55 · size) gf, antagonist step (S) = (8 − 0.04 · size) gf. Pulse height (PH) = 65 gf for 10° saccade; 120 gf for 20°. Pause height (PH) = 0.25 + exp(−size/2.5). The filter time constants = 7 ms. These parameter values were set after adjustment during simulations so that the model generated saccades of the appropriate magnitude with realistic peak velocities, within the range observed in the recorded monkey data.

The differential equations describing the model are as follows:

$$\frac{dx}{dt} = v$$

$$\frac{dv}{dt} = \frac{1}{J}\left[-K_o x - B_o v + F_{P_1} + K_{se}(y_1 - x) - F_{P_2} + K_{se}(x - y_2)\right]$$

$$\frac{dy_1}{dt} = \frac{1}{B_1}\left[F_{a1} - K_{se}(y_1 - x)\right]$$

$$\frac{dy_2}{dt} = \frac{1}{B_2}\left[-F_{a2} - K_{se}(y_2 - x)\right]$$

$$\frac{dF_{a1}}{dt} = \frac{1}{T_1}(I_1 - F_{a1})$$

$$\frac{dF_{a2}}{dt} = \frac{1}{T_2}(I_2 - F_{a2})$$

where

$$B_1 = \begin{cases} \dfrac{(F_{a1} + 0.25F_{a1})}{\left(b_H + \dfrac{dy_1}{dt}\right)}, & \dfrac{dy_1}{dt} \geq 0 \\ \dfrac{3F_{a1}}{d_{len}}, & \dfrac{dy_1}{dt} < 0 \end{cases}$$

$$B_2 = \begin{cases} \dfrac{3F_{a2}}{d_{len}}, & \dfrac{dy_2}{dt} \geq 0 \\ \dfrac{(F_{a2} + 0.25F_{a2})}{b_H + \dfrac{dy_2}{dt}}, & \dfrac{dy_2}{dt} < 0 \end{cases}$$

where $x$ (degrees) is eye position; $v$ (degrees/sec) is eye velocity; $y_1$, $y_2$ (degrees) are positions of the hypothetical nodes; $F_{a1}$, $F_{a2}$ (gf) are "active state" (*i.e.*, hypothetical isometric force); $I_1$, $I_2$ (equivalent gf) are the innervations to each muscle (pulse-step); $B_1$, $B_2$ (gf sec/deg) are the muscle viscosities; $T_1$, $T_2$ (msec) are the time constants of the input filters; $b_H = V_{max}/4$ (degrees/sec) is a constant defined by Hill (16) used to characterize the shortening force-velocity relationship of muscle; $d_{len} = b_H$ is the parameter scaling lengthening force-velocity relation. This parameter was explicitly defined because it is varied in some of the simulations (see discussion in the text). Specifically in the modified Hill model $d_{len}$ was different in the agonist and antagonist muscles: $d_{len} = 4150$ in the agonist and 450 in the antagonist.

## APPENDIX B

Zahalak's distribution moment (DM) muscle model is an approximation to Huxley's 1957 two-state cross-bridge model of sarcomere contraction. Figure 5 shows a schematic of the model. When partial activation and myosin/actin filament overlap is also considered, the following partial differential equation describes the rate of change of the cross-bridge bond distribution:

$$\frac{\partial n(x, t)}{\partial t} - v(t)\frac{\partial n(x, t)}{\partial x} = f(x)\{\alpha(t)c[s(t)] - n(x, t)\} - g(x)n(x, t)$$

where $n(x, t)$ is the bond distribution; $v(t)$ is the velocity of shortening; $f(x)$ is the rate of bond attachment; $g(x)$ is the rate of bond detachment; $\alpha(t)$ is the fraction of cross-bridge sites activated; $c[s(t)]$ is the fraction of sites in the region of actin/myosin filament overlap; $s(t)$ is the sarcomere length. The following equations result from Zahalak's derivation of the model after normalization by the maximum length ($h$) at which a cross-bridge can be formed (34):

$$\frac{dQ_\lambda}{dt} = \alpha(t)c[s(t)]\beta_\lambda - \phi_\lambda(Q_0, Q_1, Q_2) - \lambda u Q_{\lambda-1}, \quad \lambda = 0, 1, 2.$$

where

$$\xi \doteq \frac{x}{h}, \quad Q_\lambda = \int_{-\infty}^{\infty} \xi^\lambda n(\xi, t)d\xi, \quad Q_{\lambda-1} \doteq 0$$

$$\beta_\lambda \doteq \int_{-\infty}^{\infty} \xi^\lambda f(\xi)d\xi, \quad \phi_\lambda \doteq \int_{-\infty}^{\infty} \xi^\lambda [f(\xi) + g(\xi)]n(\xi, t)d\xi$$

$$p \doteq \frac{Q_1}{Q_0}, \quad q \doteq \sqrt{\frac{Q_2}{Q_0} - \left(\frac{Q_1}{Q_0}\right)^2}, \quad u \doteq \frac{v}{h},$$

with

$$n(\xi, t) = \frac{Q_0}{\sqrt{2\Pi}q} e^{-\frac{(\xi - p)^2}{2q^2}}$$

where $Q_0$, $Q_1$, $Q_2$ are the normalized moments of the Gaussian bond distribution; $\xi$ is the normalized spring length; $u$ is the normalized rate of shortening; $n(\xi, t)$ is the normalized bond distribution; $p$ is the mean of the Gaussian $n(\xi, t)$; and $q$ is the standard deviation of the Gaussian $n(\xi, t)$; $s(t)$ is the sarcomere length; $f$ (the rate of cross-bridge attachment) and $g$ (the rate of cross-bridge detachment) are described as follows:

$$f(\xi) = \begin{cases} 0, & \xi < 0, \\ f_1\xi, & 0 < \xi < 1, \\ 0, & 1 < \xi, \end{cases}$$

$$g(\xi) = \begin{cases} g_2, & \xi < 0, \\ g_1\xi, & 0 < \xi < 1, \\ g_1\xi + g_3(\xi - 1), & 1 < \xi \end{cases}$$

Muscle force is calculated from the bond distribution as follows:

$$force = \frac{ms_{PP}k}{21}\int_{-\infty}^{\infty} xn(x, t)dx = \frac{ms_{PP}kh^2A_{PP}}{21}Q_1$$

where $m$ is the number of cross-bridge sites (/cm$^3$), $s_{PP}$ is the sarcomere length in the reference state (primary position) (cm), $k$ is the cross-bridge spring constant (dyne/cm); $l$ is the distance between actin binding sites (cm); $A_{PP}$ is the cross-sectional area in the reference state (cm$^2$). The maximum isometric force at a particular length is found by solving the partial differential equation for steady-state, zero velocity condition:

$$\max force\ (eye) = \frac{ms_{PP}kh^2A_{PP}}{21}c_e\ (eye)\frac{f_1}{f_1 + g_1}$$

In addition eye velocity must be converted to normalized sarcomere velocity:

$$v = \frac{dE}{dt}\frac{\gamma}{2n_s} SGN, \quad u = \frac{v}{h}$$

where

$$\gamma = \frac{2\Pi R}{360}$$

$$SGN = \begin{cases} -1, & \textit{for medial rectus} \\ +1, & \textit{for lateral rectus} \end{cases}$$

$v$ is the velocity of shortening of the half-sarcomere [cm/s/half-sarcomere]; $n_s$ is the number of sarcomeres in one myofibril running the length of the muscle; $u$ is the normalized velocity (actin sites/sec/half-sarcomere); $R$ is the radius of the globe (cm); $\gamma$ is the a conversion factor (cm/degree); *SGN* converts the sign of velocity to positive for shortening muscle; $dE/dt$ is eye velocity (degrees/sec).

The values of the parameters we used in the DM model were derived mostly from monkey extraocular muscle data, wherever possible; however, several estimates were made from studies on other skeletal muscle. Parameters were measured directly, calculated from measured parameters, estimated to be consistent with measured muscle properties, or estimated by trial and error in simulations. All parameters estimated by simulation were determined for one saccade trajectory and then tested with other trajectories.

To simplify the comparison of the DM and Hill-type muscle models, the cross-bridge overlap function was neglected in the simulations (*i.e.*, $c[s(t)] = 1$) because the Hill-type model ignores the length-tension curve. However, it was used to estimate or verify estimates of other parameters, so its derivation will be described. This function was estimated from the length-tension curves of human LR (29) and the sarcomere length-tension curve of mammalian muscle (33). Since all sarcomeres are assumed to be identical, the plateau portion of the whole-muscle length-tension curve corresponds to the plateau region in the sarcomere length-tension curve as does the respective lengths at which the tension reaches zero. The cross-bridge function in degrees of eye rotation that results from this line of reasoning is:

$$\begin{aligned} &\textit{if } (eye < -80) \textit{ then } c_e(eye) = 0.0 \\ &\textit{else if } (eye < 25) \quad \textit{then } c_e(eye) = 0.0095\ (eye + 80) \\ &\textit{else} \qquad\qquad\qquad\quad c_e(eye) = 1.0 \end{aligned}$$

where eye is eye position relative to primary position (degree); $c_e$ (eye) is the cross-bridge overlap function, or (for both the LR and MR):

$$\begin{aligned} &\textit{if } (s_{len} < 0.7\ \mu m) \quad \textit{then } c_s(s_{len}) = 0.0 \\ &\textit{else if } (s_{len} < 2.39\ \mu m) \textit{ then } c_s(s_{len}) = 5917\ (s_{len} + 0.7) \\ &\textit{else} \qquad\qquad\qquad\quad c_s(s_{len}) = 1.0 \end{aligned}$$

where $s_{len}$ is the sarcomere length ($\mu$m); $c_s(s_{len})$ is the cross-bridge overlap function. The partially innervated active length-tension curves of whole muscle are calculated by scaling the whole length-tension curve by the level of innervation.

The muscle length at primary position, $L_{pp}$ = 1.985 cm (22); muscle cross-sectional area at primary position, $A_{pp}$ = 0.0965 cm$^2$ (22); sarcomere length at primary position, $s_{pp}$ = 1.98e−4 cm, (estimated from the cross-bridge overlap function); radius of the globe, $R$ = 0.93 ± 0.05 cm (22); cross-bridge sites per unit volume, $m$ = 5.7e16 1/cm$^3$ (18); maximum active isometric force $F_0$ = 55 gf (12); maximum active isometric force at primary position, $F_{0pp}$ = 45 gf (12); maximum force/area, $P_0$ = 670 gf/cm$^2$ (26); maximum velocity of shortening, $SV_{max}$ = 25 lengths/sec (estimated from rat inferior rectus, assuming a sarcomere length of 2.39 $\mu$m [4]); number of sarcomeres in series, $n_s = L_{pp}/s_{pp}$ = 10,025; conversion factor from degrees to cm, $\gamma$ = 0.0162 cm/deg; maximum velocity of shortening, $V_{max} = SV_{max}\, L_{pp}/\gamma$ = 3070 degrees/sec. The maximum distance over which a cross-bridge can form, $h$ = 1.85e−6 cm (18,33); energy per cross-bridge cycle, $e$ = 7e−13 erg/molecule; efficiency of cross-bridge cycle: the ratio of work to energy, $w/e$ = 0.8 (18); dimensionless ratio, which partially characterizes the force-velocity relationship of shortening muscle, $a_H/P_0$ = 0.5; dimensionless ratio, which partially characterizes the force-velocity relationship of shortening muscle, $b_H/V_{max}$ = 0.33 (18,33).

The parameters describing the rate of cross-bridge detachment and attachment were found as follows. The rate of cross-bridge detachment in region $0 < \xi < h$ and part of the rate in region $\xi > 1$, $g_1\xi$ = 425$\xi$ 1/sec for the agonist; 220$\xi$ 1/sec for the antagonist. For the antagonist the value of $g_1$ was chosen to satisfy Hill's result that the maintenance heat, $E_0 = a_H b_H$. $E_0$ is derived from the cross-bridge model.

$$E_0 = \frac{mehg_1}{21}\frac{f_1}{f_1 + g_1} = \frac{P_0 V_{max}}{6}$$

Substituting for $P_0$ in the equation for $E_0$ and solving for $g_1$ yields:

$$g_1 = \frac{V_{max}}{6h}\frac{w}{e}$$

Simulations suggested that the higher value of $g_1$ was desirable for the agonist muscle. The distance between cross-bridge sites, $l$ = 3.75e−6 cm. (An estimate of

3.5e−6 [33] was originally chosen. However, this led to an estimate of $f_1$ that was less than two times $g_1$. The value chosen was a compromise between overestimating $l$ and underestimating $f_1$ relative to $g_1$.)

The rate of cross-bridge attachment in region $0 < \xi < h$, $f_1 \xi = 950\xi$ 1/sec. This value of $f_1$ was determined solving $E_0$ for $f_1$:

$$\frac{f_1}{f_1 + g_1} = 17{,}4415l, \quad g_1 = 425$$

As a result, as the estimate of $l$ increases, so does the estimate of $f_1$. $f_1$ is usually chosen to be considerably larger than $g_1$ so the force-velocity relationship shows a non-linearity at zero velocity (18).

The rate of cross-bridge detachment in region $\xi x < 0$, $g_2 = 2200$ 1/sec. The parameter $g_2$ was adjusted so the model force approached zero as the velocity of shortening approached $V_{max}$. Huxley made the arbitrary assumption that $(f_1 + g_1)h$/sec $= b_H$ because it simplified the steady-state solution of the partial differential equation; as a result, he concluded that $g_2/(f_1 + g_1) = 3.919$. This was not done in our derivation.

We set the partial rate of cross-bridge detachment in the region $\xi < 1$, $g_3 = -425$ 1/sec for the agonist and $-220$ 1/sec for the antagonist. The value of $g_3$ was chosen such that g would be a constant in the region beyond which cross-bridges were not likely to form and piecewise continuous with the rate of detachment in the region in which cross-bridges are likely to attach (0 to 1). This parameter $g_3$ affects the force/lengthening velocity relationship.

Since $P_0 = ms_0kh^2f_1/[41(f_1 + g_1)]$ (solve the partial differential equation for steady-state, zero velocity), where $s_0$ is the sarcomere length at which the maximum developed force is achieved, the spring constant of the cross-bridges must be: $k = P_0 41(f_1 + g_1)/(ms_0h^2f_1) = 0.3$ dyne/cm; the spring constant is derived from measurements made at maximum isometric force, and, therefore, is based on $g_1$ of the agonist muscle. We have assumed that the spring constant is the same in both fiber types (slow and fast).

Integrating the equations for $\beta_0 - \beta_2$ (see model description) yields: $\beta_0 = f_1/2 = 262.5$; $\beta_1 = f_1/3 = 175$; $\beta_2 = f_1/4 = 131.25$.

## APPENDIX C

This appendix describes the method used to estimation absolute forces from the measured force profiles. Because the amplifiers were modified early in the course of the experiments (but before any of the data used here was collected), it was necessary to estimate absolute forces instead of directly calculating the absolute forces represented by the data. First, we assumed that the forces at primary position and the range of forces generated during each session were the same in the LR and MR. In humans, some data suggest the MR may exert higher forces than the LR (7); however, other data support the assumption (6,8). As of this time, the issue has not been explored in monkeys, so we will make the assumption that they are the same. Second, we assumed the force developed in monkey extraocular muscle could be estimated by scaling the force developed in human extraocular muscle by the ratio of cross-sectional areas of the two muscles. To this end, we noted that the monkey fixation force at primary position corresponded to 32.5% of the total range of forces recorded in the monkey (*i.e.*, the minimum force measurement was considered 0% and the maximum 100% (12). Then we noted that the human fixation force at primary position in the LR is, on average, about 13.7 gf (29). Moreover, the ratio of monkey to human cross-sectional area is about 0.57 (0.0965 $cm^2$ monkey [21]; 0.169 $cm^2$ human [15]). Therefore, we assumed 32.5% corresponded to 7.8 gf and scaled the force data accordingly. The assumptions made in this derivation is supported by three further observations. First, the force developed by muscles with the same fiber composition scales by cross-sectional area (for a given level of innervation). Second, the maximum active isometric force for monkey and human LR scale approximately the same as cross-sectional area (55 gf monkey [12]; 100 gf human [6]). Finally, we noted that the position dependent fixation forces recorded in our monkey scaled relative to each other just as those fixation forces recorded in the human extraocular muscle scaled relative to each other (27).